Ionospheric control of the magnetospheric configuration: Thermospheric neutral winds

A. J. Ridley
The University of Michigan, Ann Arbor, Michigan, USA

A. D. Richmond
High Altitude Observatory, National Center for Atmospheric Research, Boulder, Colorado, USA

T. I. Gombosi, D. L. De Zeeuw, and C. R. Clauer
The University of Michigan, Ann Arbor, Michigan, USA

Received 1 May 2002; revised 4 February 2003; accepted 29 April 2003; published 26 August 2003.

[1] In this study we present the first results from the University of Michigan's coupled magnetosphere-ionosphere-thermosphere general circulation model. This code is a combination of the Michigan MHD model with the NCAR thermosphere-ionosphere-electrodynamics general circulation model (TIEGCM). The MHD code provides specification of the high-latitude ionospheric electric potential and the particle precipitation pattern, while the TIEGCM provides the divergence of the height-integrated neutral wind multiplied by the conductance. This can be easily incorporated into the electric potential solver in the MHD code. We show in this study that the neutral winds cause an approximately 6% increase in the cross polar cap potential when the IMF is strongly southward. This causes the magnetospheric field aligned currents to decrease by a small amount. In the magnetosphere, the flow speeds are increased by only a small amount while the IMF is strongly southward, but when it turns northward the differences become 10–20%. When the IMF is northward, the pressure on the dayside magnetosphere is reduced while the pressure on the nightside is increased by ~10% of the total pressure. *INDEX TERMS:* 2431 Ionosphere: Ionosphere/magnetosphere interactions (2736); 2740 Magnetospheric Physics: Magnetospheric configuration and dynamics; 2753 Magnetospheric Physics: Numerical modeling; 2760 Magnetospheric Physics: Plasma convection; 2407 Ionosphere: Auroral ionosphere (2704); *KEYWORDS:* neutral winds, ionospheric convection, magnetospheric dynamics, magnetosphere-ionosphere coupling

Citation: Ridley, A. J., A. D. Richmond, T. I. Gombosi, D. L. De Zeeuw, and C. R. Clauer, Ionospheric control of the magnetospheric configuration: Thermospheric neutral winds, *J. Geophys. Res.*, *108*(A8), 1328, doi:10.1029/2002JA009464, 2003.

1. Introduction

[2] This study is part of three related studies that examine the influence of the thermosphere and ionosphere on the global state of the magnetosphere. The present study examines how the thermospheric neutral winds affect the ionospheric electric field and magnetospheric convection and pressure distribution. The other two studies examine the influence of the ionospheric conductance on the magnetospheric configuration [*Ridley et al.*, 2003] and the influence of ionospheric outflow on the time-dependent magnetospheric dynamics.

[3] The neutral wind has long been known to be coupled with the ion flow [e.g., *Axford and Hines*, 1961]. This coupling occurs through the ion-neutral collisions, which cause the neutrals to be accelerated toward the ion velocity but with a time lag of typically a few hours owing to inertia of the neutrals. In turn, the neutrals, through the ionospheric wind dynamo mechanism, can generate an electric field that has a tendency towards causing the ions to move with the neutrals. In regions where the wind-induced horizontal currents diverge, the neutrals can influence the magnetospheric convection. The inertia of the neutrals can help maintain ion convection even when the magnetospheric dynamo source of the electric field is suddenly weakened. This is known as the fly-wheel effect [*Banks*, 1972; *Coroniti and Kennel*, 1973; *Richmond and Matsushita*, 1975; *Richmond*, 1995b]. Closely related to this effect is a counteracting tendency for the ionospheric wind dynamo to drive field-aligned currents in the opposite direction from those driven by the magnetospheric dynamo source [*Lyons et al.*, 1985; *Deng et al.*, 1991, 1993; *Thayer and Vickrey*, 1992].

[4] As our physical understanding of the magnetosphere-ionosphere system increases, our need to have more accurate models of the coupled system also grows. For example, *Lu et al.* [1995] studied the thermosphere and ionosphere

0148-0227/03/2002JA009464

during the 28–29 March 1992 GEM campaign. They quantified the effects of including the neutral winds in calculating the ionospheric Joule heating, mechanical power, and electromagnetic energy dissipation using the National Center for Atmospheric Research Thermosphere-Ionosphere-Electrodynamics General Circulation Model (TIEGCM) [*Richmond et al.*, 1992] driven with high-latitude inputs from the assimilative mapping of ionospheric electrodynamics (AMIE) technique [*Richmond and Kamide*, 1988]. They found that the neutral winds can reduce the estimated Joule heating by as much as 28%. They further found that the neutral wind driven field-aligned currents can be as much as 27% of the magnetospheric generated field-aligned currents.

[5] Recently, the neutral wind influence on the magnetospheric energy dissipation into the ionosphere has been studied. *Thayer and Vickrey* [1992] concluded that the neutral wind dynamo can have a relatively large influence, in comparison with the magnetospheric dynamo, in regions near the ionospheric convection reversal boundary. *Sánchez et al.* [1998] described a time period during the January 1997 CME in which the neutral winds may have provided energy to the magnetosphere, rather than the normal condition, where the neutral winds receive energy from the magnetosphere. The study by *Thayer* [1998] describes how taking the height resolved neutral winds are quite important in determining the Joule dissipation. They presented examples of the Joule heating being enhanced (compared to the Joule heating calculated neglecting the neutral winds) at some altitudes while it is depressed at other altitudes.

[6] These types of studies are quite useful for a number of reasons: (1) they more accurately specify the energy input into the thermosphere, thus the composition and structure of the thermosphere can be better determined; (2) the energy balance between the solar wind, magnetosphere (i.e., ring current, stored energy in the lobes, etc), and ionosphere (i.e., Joule heating, particle precipitation, etc.) can be better partitioned; and (3) the feedback between the ionosphere and the magnetosphere can be better understood. This last point is the focus of the present study. In previous studies, such as those described above, the regions of Joule heating in which the neutral wind contributed significantly by either raising or lowering the heating are the regions where magnetosphere will be influenced the strongest. This does not quantify the net effects on the magnetosphere but is a good start at examining where the influence is taking place.

[7] *Forbes and Harel* [1989] examined how thermospheric winds can modify the electric fields and field-aligned currents calculated with a model of inner-magnetospheric plasma convection. Assuming that the wind velocity was a certain fraction of the plasma velocity, they showed that the winds can have effects such as an increase in the steady-state shielding of electric fields between high and low latitudes produced by the hot magnetospheric plasma. The model presented by *Peymirat et al.* [1998, 2002] showed results of a coupled TIEGCM and inner magnetosphere model. Both the thermospheric and magnetospheric response to each other were examined. These were the first studies that attempted to quantify the effects of the neutral winds on the magnetosphere in a self-consistent manner. They showed that the neutral winds can cause pressure changes of ~20% in the magnetosphere.

[8] While the studies described above have made many interesting and quite useful insights, these papers have mainly been event studies. Very few statistical studies have been conducted because of the difficulties in measuring all of the relevant ionospheric and thermospheric parameters. In addition, there have been few modeling efforts made at quantifying these parameters. While a quantification of the influence of the neutral winds on the ionospheric convection pattern and energy dissipation is lacking, a quantification of the neutral wind influence on the magnetosphere does not yet exist. This is because of the difficulty in measuring all of the ionospheric, thermospheric, and magnetospheric quantities for a number of different conditions.

[9] In this study we present a coupled model of the magnetosphere-ionosphere-thermosphere system. The model is based on the Michigan magnetospheric MHD model [*Powell et al.*, 1999; *Groth et al.*, 2000] and the NCAR TIEGCM that has been used in numerous studies of the ionosphere-thermosphere system [*Richmond et al.*, 1992; *Lu et al.*, 1995; *Emery et al.*, 1996; *Schoendorf and Crowley*, 1995; *Crowley et al.*, 1996].

2. Technique

[10] The two-way coupling between the magnetosphere-ionosphere system and the thermosphere is modeled using existing codes which are coupled together. The global magnetospheric state is solved for using the Michigan MHD model [*Powell et al.*, 1999], while the thermospheric state is solved for using the TIEGCM.

2.1. Magnetospheric Model

[11] The magnetospheric model solves the ideal MHD equations to compute the magnetic field, ion density, temperature, and velocity structure in the magnetosphere. From these quantities, currents and electric fields are derived. The outer boundaries of the code are typically put at $\pm 64\ R_e$ in the GSM Z and Y direction while X ranges from $-224\ R_e$ in the tail to $32\ R_e$ upstream of the Earth. These boundaries are of sufficient distance to not influence the magnetospheric structure. The Michigan MHD model has a tilted, rotating dipole, which is consistent with the Earth's dipole. Recently, the MHD model has been validated in two studies that show how the results correlate with observations [*Ridley et al.*, 2001; *Ridley et al.*, 2002]. The ionosphere is coupled to the MHD code in a similar manner as that described by *Goodman* [1995]. The field aligned currents at $3.5\ R_e$ are derived from $\nabla \times \mathbf{B}$. These currents are mapped down to the ionosphere using the intrinsic magnetic field within the code, and the current densities are scaled by the ratio of the magnetic field in the ionosphere to that in the magnetosphere. The currents are combined with a conductance pattern to solve for the potential. This potential pattern is mapped up to the magnetospheric inner boundary at $2.5\ R_e$, assuming no field-aligned potential drop. Corotation velocities are determined and added to the convection velocities derived from the potential pattern and magnetic field. These combined velocities are applied as the inner boundary condition in

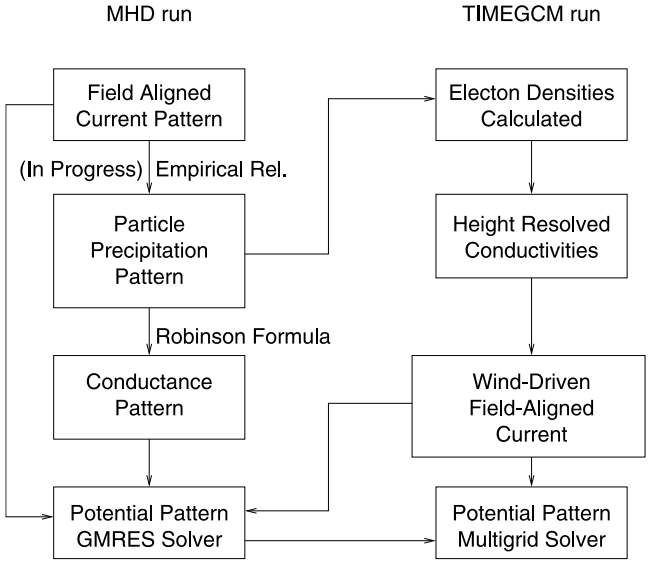

Figure 1. The flow pattern of the coupled MHD-TIEGCM Model.

the MHD model. The applied velocities push around the plasma and magnetic field, which then alters the pressure distribution and field-aligned currents flowing into the ionosphere. Taking this feedback into account, the magnetosphere acts as neither a current generator nor a voltage generator exclusively [*Fedder and Lyon*, 1987; *Ridley et al.*, 2003a].

[12] The precipitation pattern used in the potential solver is derived from the field-aligned current structure such that an auroral oval is produced. The precipitation dependence is described further by *Ridley et al.* [2001] and *Ridley and Liemohn* [2002]. The *Robinson et al.* [1987] formulation is used to convert the precipitation pattern to an auroral conductance pattern. A solar EUV generated conductance [*Moen and Brekke*, 1993] as well as a polar cap precipitation and a uniform conductance are added to the auroral conductance. The uniform conductance is created by star light, cosmic rays, and other approximately uniform sources. In addition, the F-region ionospheric loss rates are such that there is a small electron density sustained throughout the night time. It is estimated that the uniform conductance adds 0.25 (0.5) mho Pedersen (Hall) constant conductance across the globe.

2.2. Thermosphere-Ionosphere Model

[13] The TIEGCM solves for the thermospheric and ionospheric composition, temperature, and winds. The model solves for mass mixing ratios of the neutral major species O_2, N_2, and O and the minor species N(^2D), N(^4S), NO, He, and Ar. For the ions the O^+ dynamics are considered, while the species O_2^+, N_2^+, NO^+, and N^+ are considered to be in photochemical equilibrium. The TIEGCM is a full three-dimensional code with 5° latitude by 5° longitude by 0.5 scale height altitude cells. There are 29 pressure levels within the model such that the simulation spans from ~95 km to 650 km in altitude.

[14] The electrodynamics within the TIEGCM focus on the middle and lower latitudes, with a self consistent calculation of the interaction between the neutral winds, currents, and electric fields. At the high latitudes an external electric field is specified. Typically, an empirical electric potential model such as that by *Heelis et al.* [1982] or the potentials calculated by AMIE are used. In this case the potentials derived from the MHD code are used at high latitudes. These specified high-latitude potentials affect the neutral dynamics through ion drag and Joule heating but are not influenced by the ionospheric wind dynamo within the TIEGCM. The influence of the neutral winds on the high-latitude potential pattern is considered in the MHD code (as described below). A transition region exists in which the TIEGCM linearly scales the electric potential between the (specified) high and (self-consistently calculated) middle and low-latitude regions. The electrodynamics of the TIEGCM are solved on a magnetic apex grid based on the 1985 International Geomagnetic Reference Field [*Richmond*, 1995a].

[15] The main auroral electron precipitation is specified at high latitudes using an external model [*Roble and Ridley*, 1987], or in this case, the precipitation pattern

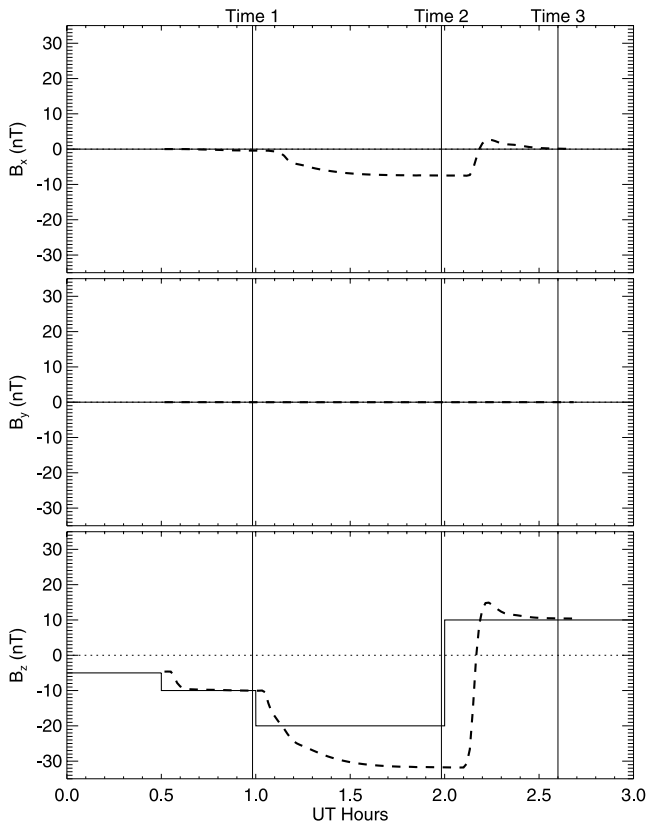

Figure 2. The solid lines show the interplanetary magnetic field (IMF) used in the simulations, while the dashed line shows the value on the *X*-line at ~12 R_e. The solar wind density, velocity, and temperature were held constant at 5 AMU/cm^3, (−500,0,0) km/s, and 1.8 × 10^5 K, respectively. The dashed line has some *X* component because the magnetopause moves close to the Earth when the IMF becomes strongly southward in combination with the dipole-tilt of the model. The vertical lines show the time periods which will be discussed in the proceeding plates.

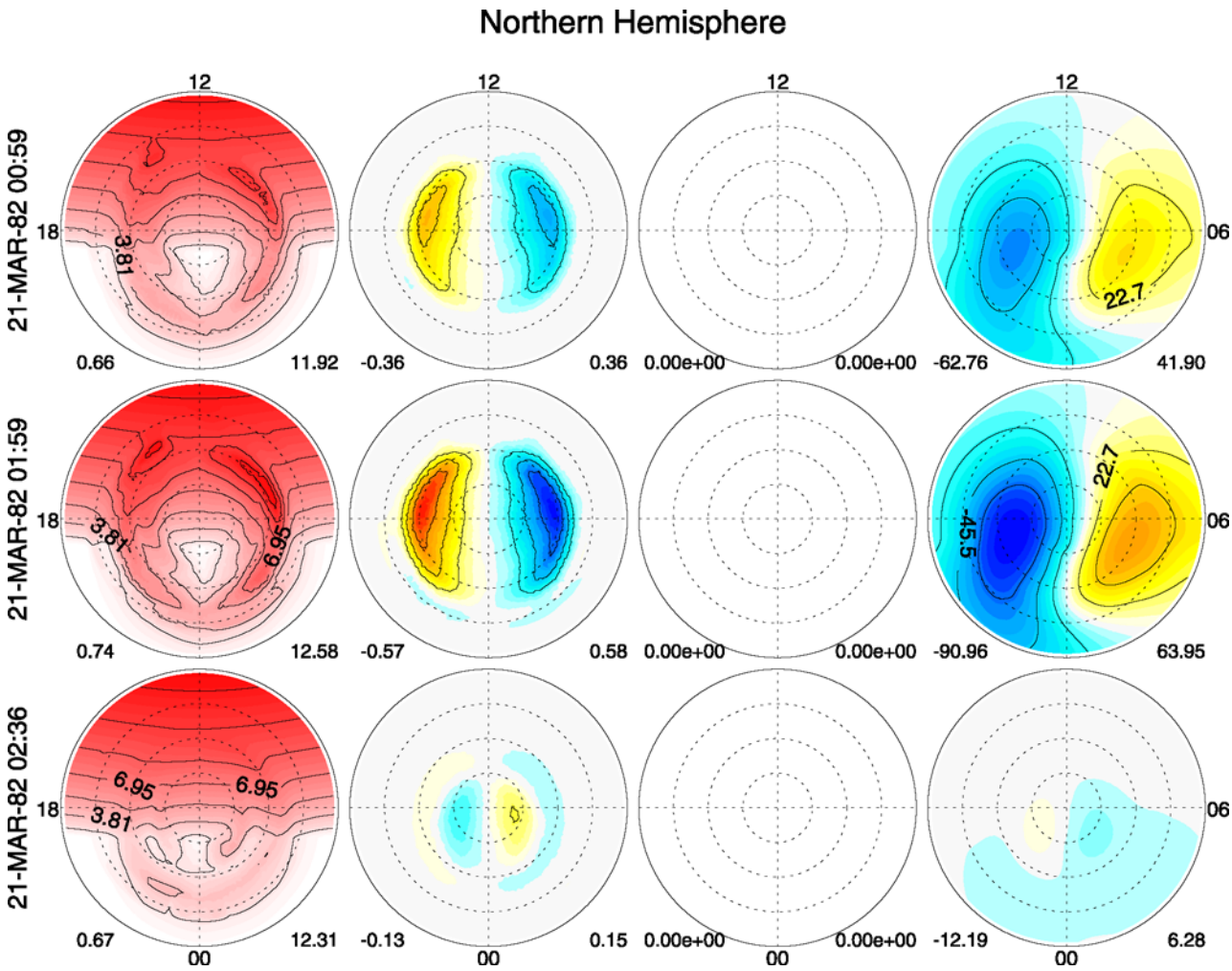

Figure 3. The results from the MHD-only simulation at ionospheric heights at the times shown in Figure 2. From left to right: Pedersen conductance (in *mhos*), radial current from the MHD code (in $\mu A/m^2$), radial projection of the wind-driven FAC obtained from the thermosphere-ionosphere code (which is zero in the MHD-only simulation), and the resulting electric potential pattern (in *kV*). Each plot is shown with the north magnetic pole at the center, and 50° magnetic latitude as the outer ring. Noon is located towards the top of the plot, while dusk is to the left. The minimum and maximum values are shown to the lower left and lower right of each plot, respectively.

derived from the MHD code. In addition to the main oval a polar cap precipitation is specified as well as a spatially limited cusp precipitation. These precipitation patterns are used to generate three-dimensional ionization rates and therefore strongly control the electron density at high latitudes.

2.3. Coupled Model

[16] The electric potential in the ionosphere adjusts in such a way that the three-dimensional current density remains divergence-free. Since the potential along geomagnetic field lines is essentially constant owing to the very large parallel conductivity, one can speak of a balance between the divergence of the current density perpendicular to the geomagnetic field, integrated along the geomagnetic field line from the base to the top of the ionosphere, with the field-aligned current density at the top of the ionosphere. The perpendicular current is driven both by the electrostatic field and by the neutral wind, which moves the conducting medium through the geomagnetic field. Convergence of the wind-driven perpendicular current, integrated along the geomagnetic field, contributes to the total field-aligned current (FAC) at the top of the ionosphere. Therefore, we call the convergence of field-line-integrated wind-driven perpendicular current the "wind-driven FAC." It is the difference between the total FAC coming from the magnetosphere and the wind-driven FAC that creates the electric potential. The electric field associated with the potential drives the remaining ionospheric current needed to close the total FAC. Thus to couple the magnetospheric and thermospheric/ionospheric models, we subtract the wind-driven FAC from the total upward field-aligned current when solving for the potential in the MHD model. Ideally, the same potential would be used in both models. However, because of different grids, boundary conditions, and assumptions used in the two models, there are presently two separate solvers for the potential, and thus the potentials are not identical. In the MHD model the ionospheric

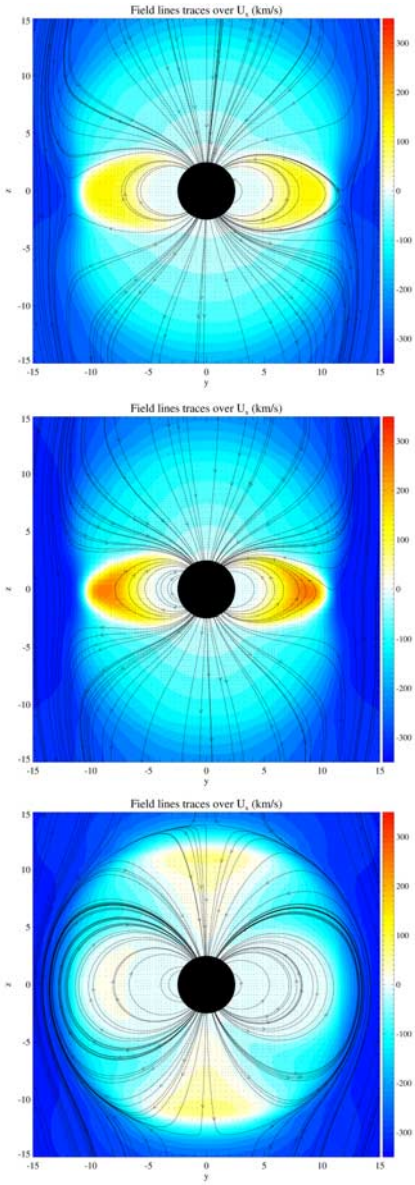

Figure 4. These plots show the magnetospheric configuration in the $X = 0$ plane. The magnetic field lines (assuming $B_x = 0$) are shown over the velocity in the X direction (with positive being towards the Sun, in units of kilometers per second). The three times shown are those indicated in Figure 2 (from top to bottom).

potentials for each hemisphere are solved for separately. This means that instantaneous patterns may have closed field lines with different potentials, but the MHD code quickly compensates to create nearly equal potentials at both footpoints of the field line. This also allows for open field lines in the different hemispheres to have different potentials. The MHD code has a lower latitudinal boundary condition of zero potential at 5° equatorward of the most equatorward field-aligned current. Within the TIEGCM the electric potential is calculated in a single hemisphere with the Northern and Southern Hemispheric conductances and neutral wind driven currents summed. The resulting potential is then applied to the different hemispheres equally, such that there are no field-aligned potential drops. Figure 1 shows which fields are passed between the models described in the previous section and how these fields are used in the models. In the coupled code the high-latitude potential is solved for in the MHD code with the GMRES solver, while the middle and low-latitude potential is solved for in the TIEGCM using a different solver. In the MHD code the middle and low-latitude potentials from the TIEGCM are ignored, since they do not map out to the MHD domain. In the TIEGCM the MHD potential solution is used at high latitudes, as described above.

[17] As described above, the MHD model has a time step of ~0.01 seconds and is highly dependent on the grid

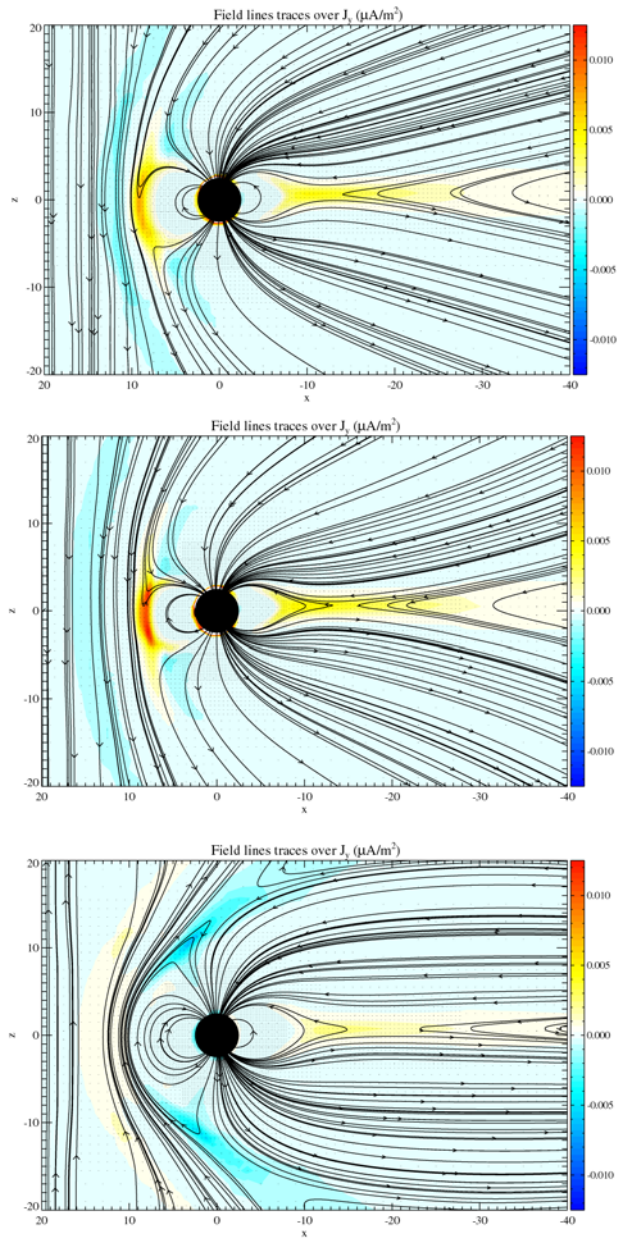

Figure 5. These plots show the magnetospheric configuration in the $Y = 0$ plane. The magnetic field lines (assuming $B_y = 0$) are shown over the current in the Y direction. The three times shown are those indicated in Figure 2 (from top to bottom).

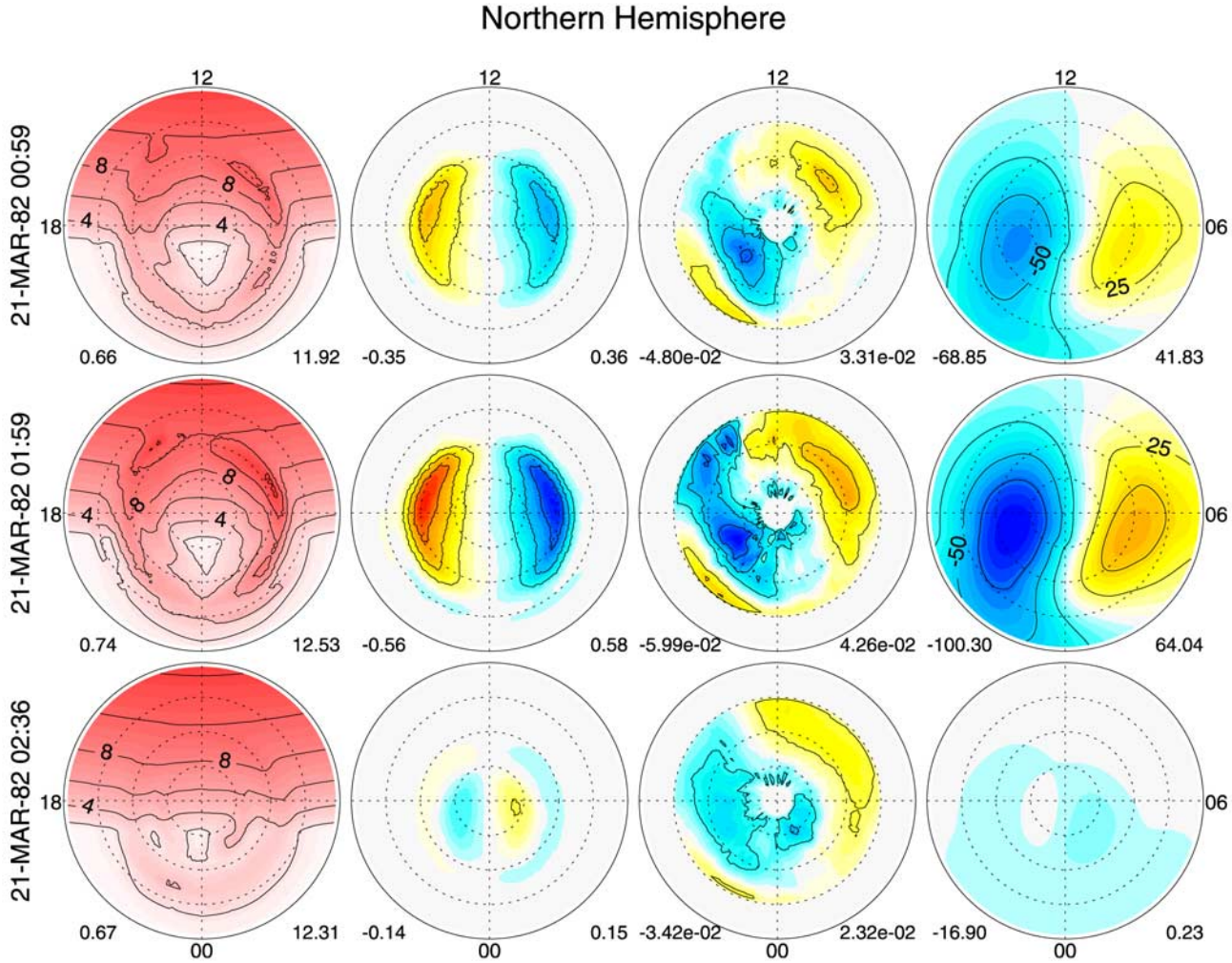

Figure 6. The results from the coupled MHD-TIEGCM simulation at ionospheric heights at the times shown in Figure 2 in the same format as Figure 3. In this instance the radial projection of the wind-driven FAC is shown.

structure. The ionospheric boundary condition is considered to be electrostatic and is calculated every 5 s. The TIEGCM, on the other hand, has a typical time step of 60–300 s. Therefore coupling between the models need only occur every 12th to 60th time that the ionospheric boundary condition is calculated. When the coupling occurs, the ionospheric potential pattern (calculated 5 s before) and electron precipitation pattern (from the current time step) are fed into the TIEGCM. The electon precipitation is used to determine the nightside ionization in calculating the electron density (see *Roble and Ridley* [1987] for details). Collision rates between ions and neutrals are then used to calculate the conductivities and the ion-drag coefficients. Only neutral-wind-driven currents above 60° are considered in the calculation of the electric potential used in the MHD model, while those below are ignored.

[18] The conductances are not consistent between the two models. The reasoning for not using the TIEGCM calculated conductances in the MHD model is that the grid size in the TIEGCM (5° latitude by 5° longitude) is too large. The auroral zone is ill represented by the TIEGCM. Because the particle precipitation is calculated by the MHD model and the conductances derived from *Robinson et al.* [1987] closely match those derived by models such as the TIEGCM, it was decided that it would be better to use the high-resolution conductances from the MHD model than the low resolution conductances from the TIEGCM. Once the resolution of the TIEGCM is increased, a more self-consistent coupling can occur.

[19] This lack of self-consistency decouples the codes in a number of different ways. For example, (1) the electric fields calculated by the MHD solution may be different than what would be expected for the derived conductances in the TIEGCM, and (2) the TIEGCM electric fields tend to be weaker than the fields from the MHD potential solver in the transition region between the polar and midlatitude regions. This implies that the ion-drag-driven neutral winds are most likely underestimated within the TIEGCM.

3. Results

[20] To demonstrate the two-way coupling between the thermosphere and the magnetosphere-ionosphere systems, two model runs were performed: a coupled MHD-

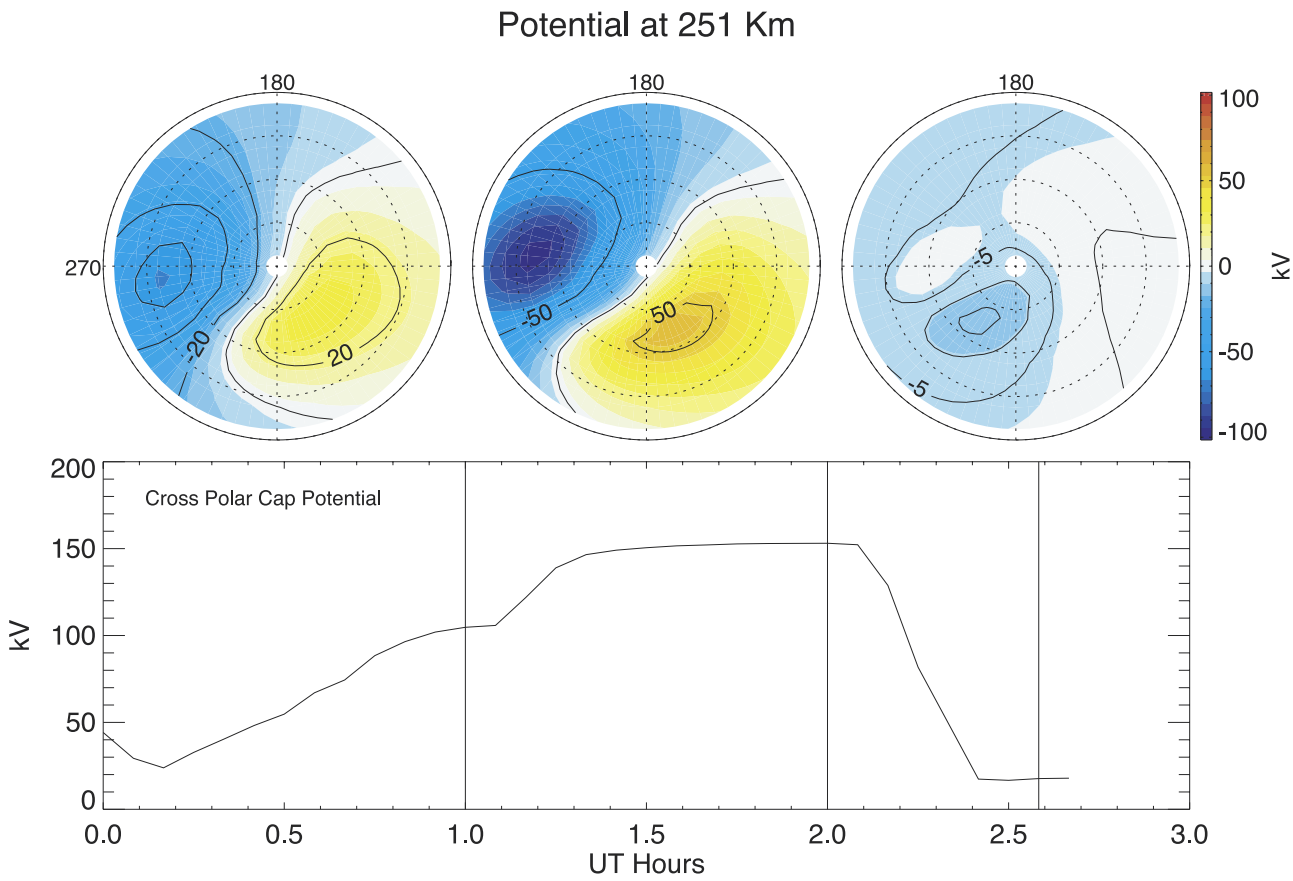

Figure 7. These plots show the ionospheric potential pattern in the geographic coordinate system within the TIEGCM at the times indicated in the lower plot by vertical lines. The center of each plot is the geographic north pole, while the outer ring is 50° geographic latitude. 180° geographic longitude is at the top of each plot, while 270° longitude is to the left. The bottom plot shows a time history of the cross polar cap potential of the Northern Hemisphere.

TIEGCM run and a stand-alone MHD run with a two-dimensional conducting ionosphere. Each was run with exactly the same upstream conditions, which are described in Figure 2. The side wall boundary conditions (i.e., zero-gradient) as well as the downstream boundary condition (i.e., zero-gradient with a low pressure) were the same between the runs also. For the inner boundary condition, the density and temperature were held constant at 100 AMU/cm^3 and 25,000 K, respectively. In the ionosphere the particle precipitation was allowed to vary between the runs, since it is specified by the magnetospheric field-aligned currents. The interplanetary magnetic field (IMF) variations which were used as inputs were aimed at driving strong field-aligned currents into the ionosphere for a limited time and then reversing them to quantify the effects of the neutral winds on the magnetospheric configuration. The negative IMF B_z tends to drive high cross polar cap potentials in the ionosphere, which serves to accelerate the neutral winds. The northward turning at 2 hours into the simulation reduces the ionospheric potential, such that in the run with MHD only, the convection in the inner magnetosphere will be substantially reduced. In the coupled run the enhanced neutral winds should serve to continue to drive flows within the inner magnetosphere, although it is expected that they will be somewhat reduced. This is the basic concept of the "fly-wheel effect" [*Banks*, 1972, *Coroniti and Kennel*, 1973].

3.1. MHD-Only Run

[21] Figure 3 shows the ionospheric results for the run with the stand-alone MHD model (assuming an ionospheric altitude of 110 km). As the IMF B_z becomes more southward, the field-aligned currents increase, which causes the conductance to increase. Since the field-aligned currents increase much more than the conductance, the potential increases significantly. After B_z turns positive the potential decreases dramatically and the high-latitude potential reverses in sign. This behavior is what is expected for the ionospheric potential for this type of time series of IMF [*Ridley et al.*, 1998, 2000].

[22] Figures 4 and 5 show the magnetospheric response to the IMF time-series. In Figure 4 the magnetic field line traces within the plane are shown. The color contours are of the velocity in and out of the plane, with positive being out of the plane (i.e., toward the Sun). The top two plots are during the B_z south period, while the bottom plot shows the magnetosphere during the B_z north period. The top plots show that the high-latitude field lines are tied directly to the IMF, which is moving antisunward. The low-latitude field lines are closed and are moving sunward. In the bottom

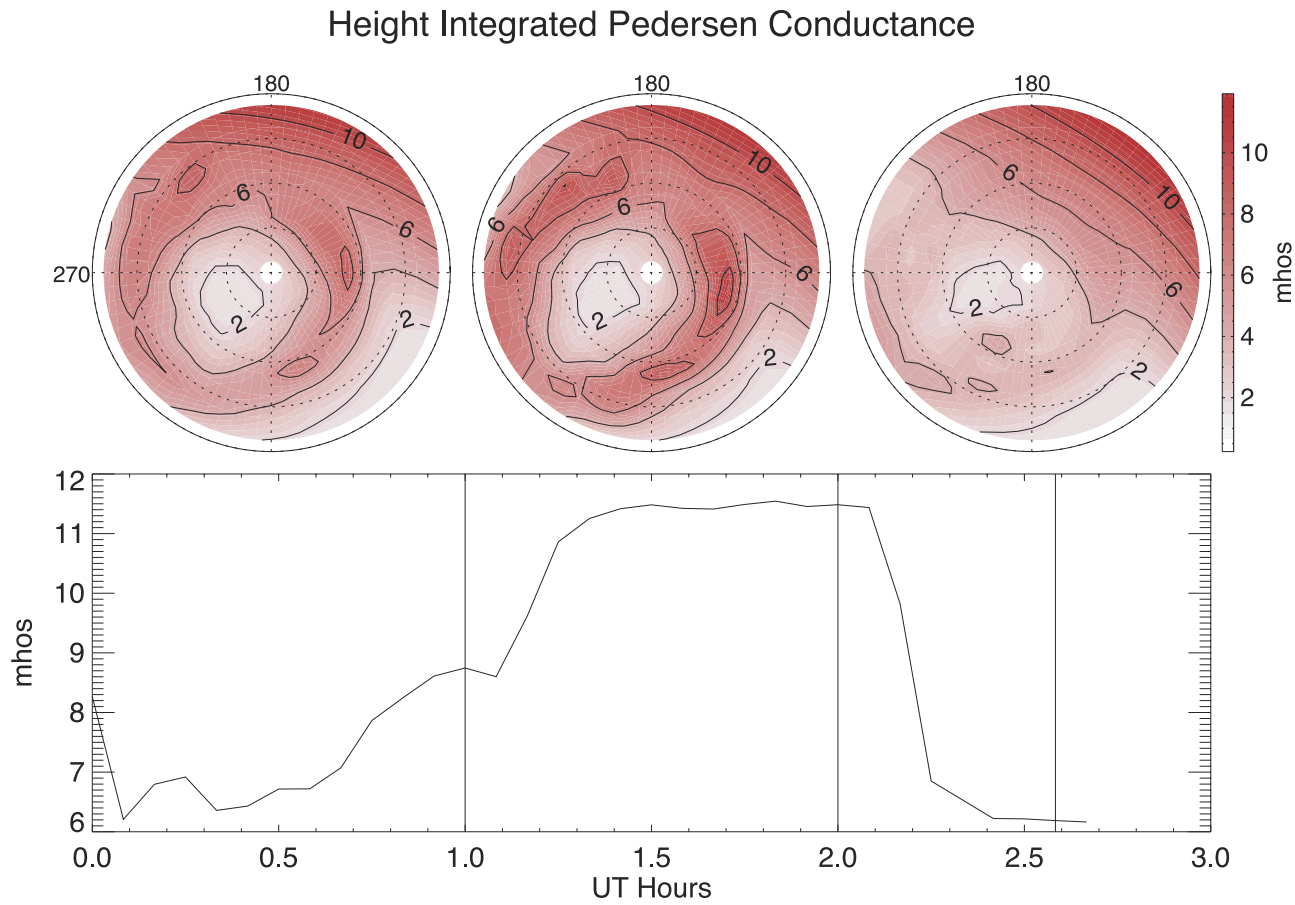

Figure 8. These plots show the height integrated ionospheric conductance in the same format as Figure 7, except the lowest latitude is 30° instead of 50°. The time history in this case is of the maximum conductance within the auroral oval.

plot the high-latitude field lines are closed, as are the low-latitude field lines. The flow in this case is very different than in the southward IMF case in that the high-latitude field lines are moving sunward and the low-latitude field lines are moving antisunward. The magnetospheric flow speeds are also significantly reduced.

[23] Figure 5 shows the magnetosphere in the $Y = 0$ plane. These plots show field line traces over the current in and out of the plane (with positive being out of the plane). As the IMF becomes more southward, the currents along the magnetopause and in the tail become larger. While it is difficult to see in these plots, the dayside magnetopause moves Earthward after the IMF change (i.e., the location of the maximum currents is closer to the Earth). After the IMF turns northward, subsolar merging stops and merging above the cusps begins, effectively closing the magnetosphere. The currents diminish significantly, and a reversed current is formed on the sunward side of the reconnection site.

3.2. Coupled Run

[24] The sequence of events described above (Figures 3, 4, and 5) is observed both in the coupled and MHD only runs. The main difference is the small amount of forcing which the neutral winds cause.

3.2.1. Ionosphere Results

[25] Figure 6 shows the ionosphere plots with the coupled code. In this case the wind-driven FAC is included. It is shown on a different scale than the total field-aligned current, with the wind-driven FAC being ~10% of the total field-aligned current, until the last time period, in which it increases to ~20%. The percent differences are the maxima of each compared. Locally, where the total field-aligned current density goes to zero, the wind-driven FAC may be dominant and the percent differences may be much larger.

[26] The ratio of the wind-driven FAC to the total field-aligned current is similar to the results presented by *Lu et al.* [1995] and *Deng et al.* [1993]. However, the pattern of the wind-driven FAC near dusk is different in the study by *Deng et al.* [1993] compared with both the study by *Lu et al.* [1995] and the results presented here: the lowest-latitude upward wind-driven FAC is more on the dayside in the study by *Deng et al.* [1993], while both the study by *Lu et al.* [1995] and the study presented here have the wind-driven FAC much further on the nightside. Because each of the three studies examined different time periods under different IMF conditions, it is almost impossible to directly compare the detailed features of each study's results. One large difference is clear, though: the magnitudes of the total field-aligned current and of the wind-driven FAC in this study are approximately a factor of 3 lower than the other two studies. For example, *Lu et al.* [1995] reported 1.81 $\mu A/m^2$ as the largest total current and 0.217 $\mu A/m^2$ as the largest wind-driven FAC, while the study presented here has 0.58 $\mu A/m^2$ and 0.06 $\mu A/m^2$ as the magnitudes of the

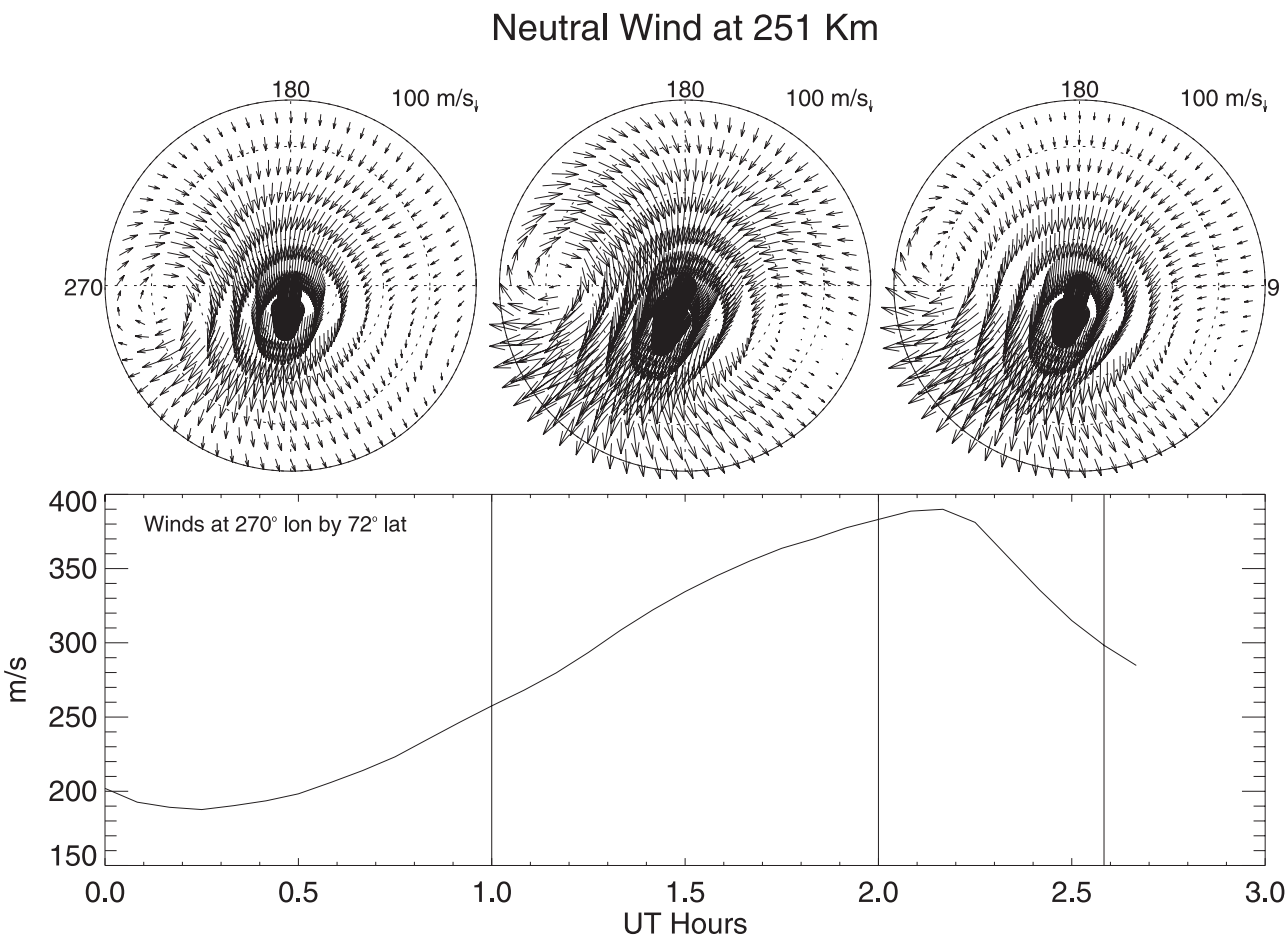

Figure 9. The neutral wind flow patterns at 251 km in the same format as Figure 7. The time history shows the wind speed at 270° longitude by 72° latitude.

total current and wind-driven FAC, respectively. The *Deng et al.* [1993] study reports similar values as the *Lu et al.* [1995] study. We have no explanation for why the magnitude of the currents would be off by such a large amount. The ratio between the two is the most important factor, though, since this determines the influence of the neutrals on the magnetosphere. The ratios are consistent, implying that the influence is most likely consistent also.

[27] In comparing the electric potential patterns between Figures 3 and 8, the electric field is stronger in the coupled run. This is because the wind-driven FAC tends to oppose the total FAC, such that the electric-field-driven current must increase to overcome the contrary wind-driven current, and thus the electric field must increase. The reason for this becomes clear when one considers the ion velocity with and without a neutral wind. When the neutral wind velocity is not considered, it is the same as assuming that the ions are moving through a stationary medium. Once this medium is allowed to move along with the ions, the drag on the ions reduces. This is not true of the electrons, since in the E-region the electron-neutral collision frequency is low compared with the electron gyrofrequency. The reduction on the drag of the ions acts like a reduction in the Pedersen conductance (see, for example, *Song et al.* [2001]). *Ridley et al.* [2003] showed that a reduction in the Pedersen conductance will raise the electric potential and will reduce the field-aligned currents. In this case, the change in cross polar cap potential was 9.4 kV, or 6.1% for the 0159 UT pattern.

[28] When the IMF turns northward, the trend is reversed in the dusk sector, but is the same in the dawn sector at high latitudes. This causes the positive cell to become dramatically reduced in size in the coupled run but reinforces the negative cell. This is more evident when comparing the wind-driven FAC with the total field-aligned currents. Where they are a different (the same) color, the electric field will be reinforced (reduced). The complex pattern of the wind-driven FAC shows that the simple picture of neutrals following the ions may be an oversimplification. Because the neutral winds are influenced by the coriolis force, upward propagating tides, viscosity, and day-to-night pressure gradients, as well as by ion-neutral drag, the neutral wind patterns are not trivial to predict, even at high latitudes [*Killeen and Roble*, 1984].

3.2.2. TIEGCM Results

[29] Figure 7 shows the Northern Hemisphere ionospheric potential pattern within the TIEGCM. Because the potential pattern is in a Sun-fixed coordinate system, while the plot is in a geographic coordinate system, it is rotating as time progresses. In addition, the potential pattern is centered on the magnetic pole, so in Figure 7 it is offset from the geographic pole by $\sim$11°. The plots show that the patterns

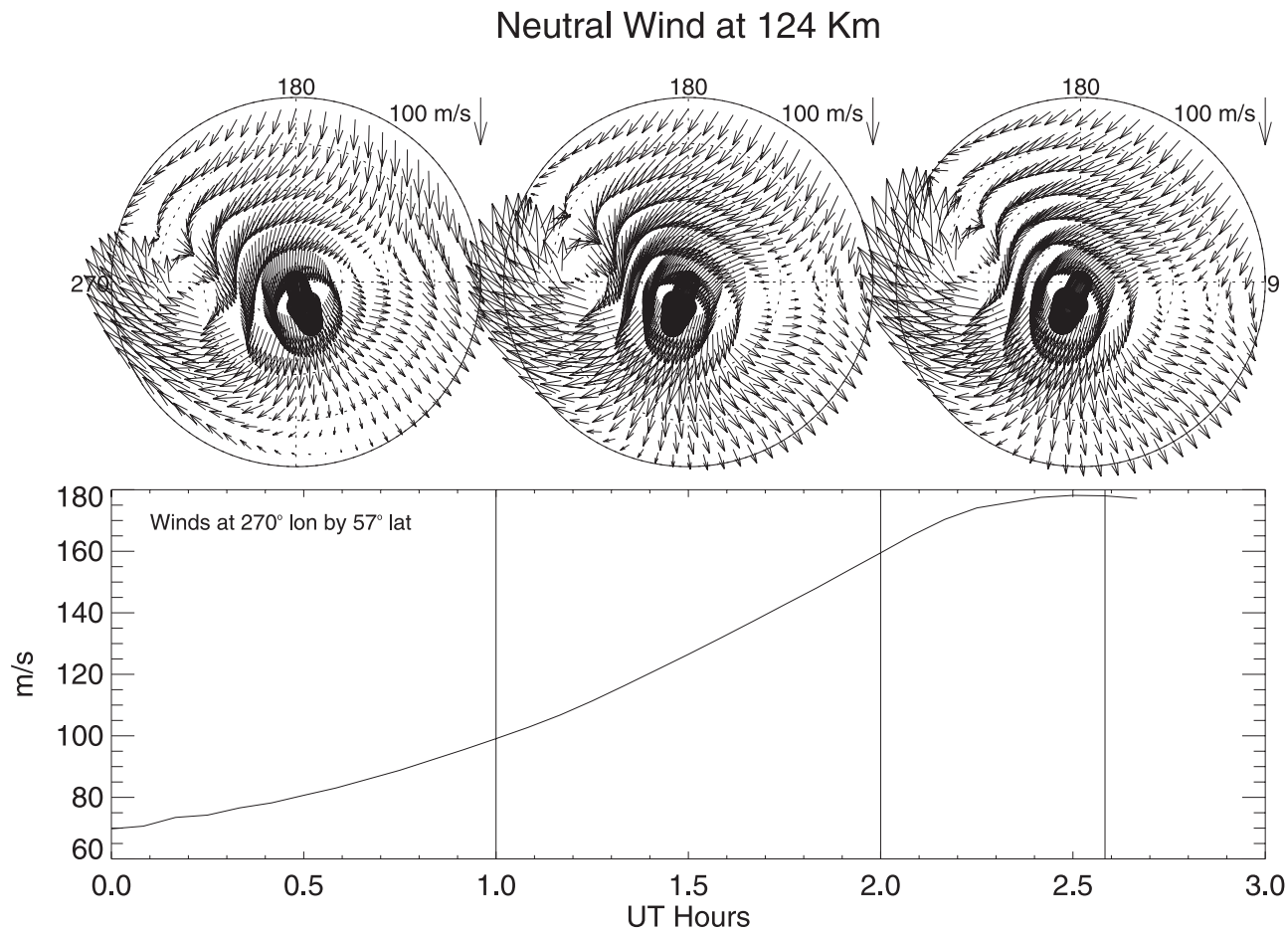

Figure 10. The neutral wind flow patterns at 124 km in the same format as Figure 9. The time history shows the wind speed at 270° longitude by 57° latitude.

match those shown in Figure 6, once they are transformed into geographic coordinates and interpolated onto a 5° by 5° grid. The time history of the cross polar cap potential matches what one would expect with the IMF shown in Figure 2. This is the same high-latitude potential pattern which is used in both the MHD code and the TIEGCM, although they are used in different coordinate systems.

[30] Figure 8 shows the height-integrated Pedersen conductance. These plots are comparable to the conductances shown in Figure 6. This shows that the electron precipitation pattern specified by the MHD code is being used to generate ionization rates within the TIEGCM which are consistent with those predicted by the *Robinson et al.* [1987] formulation. In addition, the maximum auroral Pedersen conductance plot shows the precipitation is increasing dramatically when the IMF becomes more southward and reducing substantially when the IMF turns northward, as it does in the MHD code. Small differences exist between Figures 5 and 8: (1) the TIEGCM patterns are smoother, (2) the minimum Pedersen conductance is just under 2 mhos in the TIEGCM while it is approximately 0.5 mhos in the MHD code, and (3) the solar conductance in the MHD code appears to be slightly larger than that within the TIEGCM. While these differences are quite small, they may play an important role and should be resolved.

[31] The neutral wind patterns at two different altitudes are shown in Figures 9 and 10. Note that the scales are different between the two figures. A two-cell pattern is clearly evident in the upper neutral wind patterns but is more difficult to see in the lower patterns. Both clearly show antisunward flow over the pole, which is in the same direction as the ion flow for the first two times. The neutral winds react to the changes in ion flow faster at higher altitudes than at lower altitudes. This is indicated in the time series plots, which show the neutral wind speed at a fixed latitude and longitude. At higher altitudes, the rate of change of the speed is much more dramatic (almost 100% in 2 hours) than at lower altitudes (~25% in 2 hours).

3.2.3. Magnetospheric Results

[32] Figures 11 and 12 illustrate the influence of the thermospheric neutral winds on the magnetospheric convection and pressure distribution. In Figure 11 the differences in flow in and out of the page are shown. These plots are differences between the run with coupling and the MHD-only run. Positive values indicate that the coupled run had more positive (or less negative) flows than the stand-alone MHD run. In each of the three times the difference in flow in the dusk sector (i.e., the right side of the plots) on closed field lines is positive. This indicates that in the first two cases, the flow is increased by ~5 km/s (or ~1.5% compared with the maximum flow speed). The

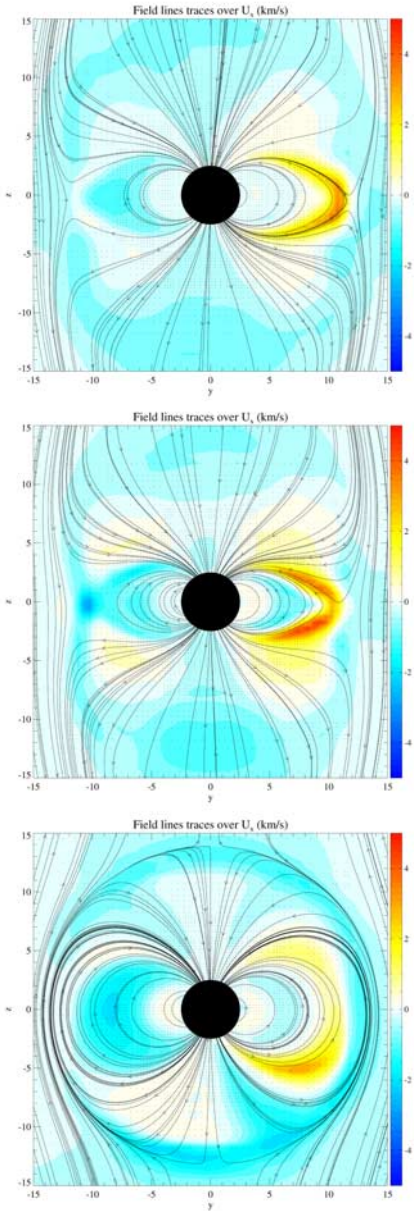

Figure 11. The difference in V_x between the run with coupling and without coupling, shown in the same format as Figure 4. Note that the color scale is different than Figure 4.

largest differences occur in the region of transition from sunward to antisunward flow. This implies that the differences may be due to the magnetosphere being slightly larger for the coupled run (on the dusk side) so that the region of sunward flow extends slightly into the region of antisunward flow in the stand-alone MHD model. On the dawnside the magnetosphere may not be any larger and may in fact be slightly smaller, since the difference is in the antisunward direction.

[33] In the final time, the flow is decreased (since in this case, the overall flow is antisunward) by $\sim$3 km/s (or $\sim$10–20%). Because this region is so far from the open-closed boundary, this is not due to an increase or decrease in the size of the magnetosphere, and is due to the direct influence of the neutral winds. This pattern mimics the ionosphere pattern, with the dusk side flow being reduced significantly.

[34] Figure 12 shows the difference in the pressure between the coupled and MHD only run, such that positive (negative) regions are those in which the pressure is enhanced (reduced) in the coupled run. All three of these difference plots indicate that the coupled magnetosphere on the dayside is enlarged, while the nightside magnetosphere is compressed with respect to the MHD-only run.

[35] The largest differences in pressure on the dayside in the first two time periods occur at the magnetopause and cusp and show that there is an outward motion of the low pressure inner magnetosphere into the cusp and out into the

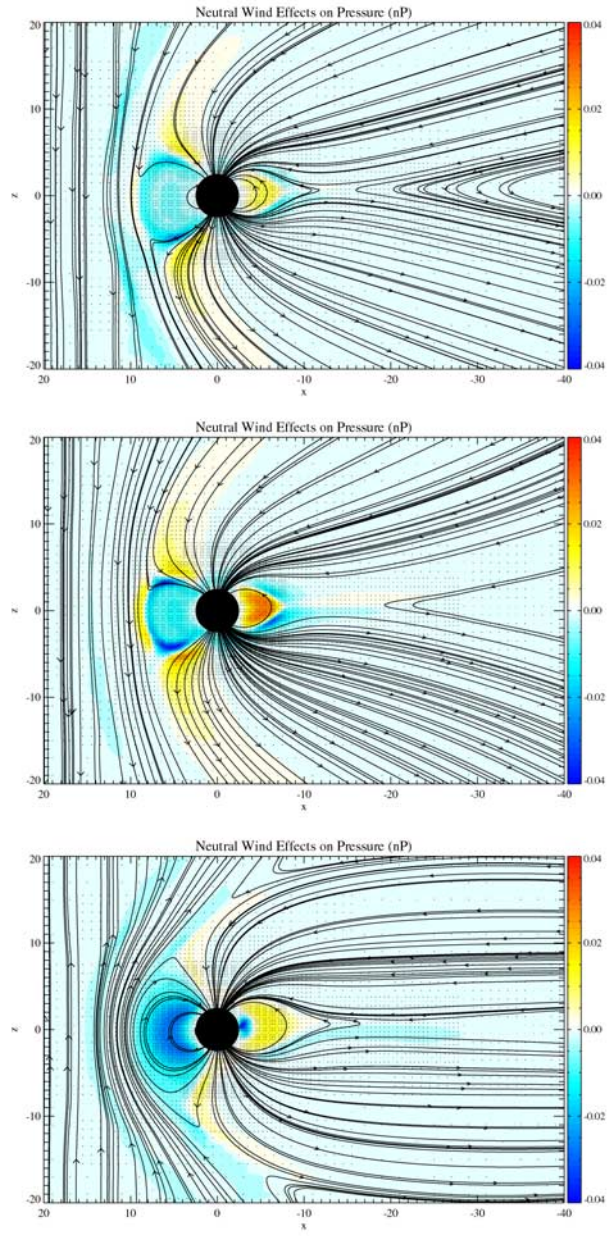

Figure 12. The difference in pressure between the run with coupling and without coupling, shown in the same format as Figure 5.

magnetosheath (with respect to the MHD-only run). On the nightside the differences in the first two time periods indicate that the higher pressure plasma sheet is populating the inner magnetosphere in the coupled run more than in the MHD-only run.

[36] Under northward IMF the pressure in the dayside inner magnetosphere is typically larger than for southward IMF. This is because the flow of the plasma at the subsolar magnetopause is antisunward, which allows magnetosheath plasma to directly enter and populate the dayside magnetosphere. A reduction of this pressure (as shown in the last plot in Figure 12) indicates that the entry of plasma has been decreased. This is most likely caused by the reduction of the velocity near the dayside magnetopause, caused by the neutral wind. On the nightside magnetosphere when the IMF is northward, the inner magnetosphere has a larger pressure than the outer magnetosphere. This is because the flux tubes are expanding as they move towards the reconnection sites above the cusp. The expansion causes the density to decrease, since the total flux tube volume should be conserved, and therefore the pressure decreases. If that expansion is slowed, the pressure will increase, which is what is indicated in the final plot in Figure 12.

4. Conclusions

[37] This study describes the coupling of a MHD model of the magnetosphere to a first principles model of the thermosphere and ionosphere system. This coupling is done by feeding the high-latitude potential and particle precipitation patterns from the MHD model to the TIEGCM, while the TIEGCM feeds the MHD code the convergence of the field-line-integrated perpendicular wind-driven current or "wind-driven FAC." The MHD model uses the wind-driven FAC to alter the high-latitude potential pattern, which is then fed back into the TIEGCM. The TIEGCM self-consistently solves for the electric fields at low latitudes, which are driven by the neutral wind dynamo, but uses the MHD provided potential pattern at the high latitudes. The conductances are not self-consistent between the two models, but the same precipitation pattern and $F10.7$ is used to drive the conductances in each code. For the study presented here the IMF B_z was held at -20 nT for about 1 hour and then suddenly changed to 10 nT. If the IMF were changed in a different way or were held constant for longer, the results may be significantly different. Consideration of the maximum effects of the neutral winds on the magnetosphere, using this coupled model, are outside the scope of the present study but may be considered in future efforts.

[38] This is one of the first studies which shows quantitatively what the influences of the ionospheric neutral winds are on the magnetospheric configuration. We show in this study that the neutral winds cause an approximately 6% increase in the cross polar cap potential when the IMF is southward. This increase causes the magnetospheric field aligned currents to decrease by a small amount. For northward IMF the current patterns become more complex, with a strong difference between the dawn-side and dusk-side currents. On the duskside the wind-driven FAC opposes the NBZ currents from the magnetosphere, such that the reversed convection in the ionosphere is reduced or could possibly overwhelm the magnetosphere-driven currents and could cause a B_z negative type of convection pattern. On the dawnside the wind-driven FAC is in the same sense as the NBZ currents and serves to enhance the reversed convection, although not as much as it is reduced on the duskside. These results show that when the IMF has been strongly southward for about an hour and the IMF turns northward, the ionospheric convection is not changed dramatically from what is expected from a stand-alone MHD simulation. If the simulation were run for a few more hours or using a stronger southward IMF, the neutral winds may show a much stronger influence.

[39] In the magnetosphere the flow speeds are increased by only a small amount while the IMF is southward, but once it turns northward the differences become 10–20%. The inclusion of neutral winds also causes the slight increase in size of the dayside magnetosphere (during southward IMF), which is indicated by the difference in pressure and the compression of the magnetosphere (also during southward IMF) on the nightside. When the IMF turns northward, the pressure on the dayside magnetosphere is reduced while the pressure on the nightside is increased. During the northward IMF periods the increases and decreases in pressure are $\sim$10% of the total pressure. These types of changes in pressure were observed by *Peymirat et al.* [1998, 2002], although they concentrated mostly on studying the nightside pressure and not the flow velocities or the dayside magnetosphere. In addition, the magnetospheric model considered by *Peymirat et al.* [1998, 2002] is an inner magnetospheric model with no consideration of the outer magnetosphere. It is encouraging that using these two different types of magnetospheric models results in similar differences in the magnetosphere, when the neutral winds are taken into account.

[40] **Acknowledgments.** This research was supported at the University of Michigan by NSF (grants ATM-9802149 and ATM-9980078) and the DoD MURI program (grant F4960-01-1-0359), and at HAO by ADR: NASA Sun-Earth Connection Theory program. The National Center for Atmospheric Research is sponsored by the National Science Foundation.

[41] Lou-Chuang Lee thanks Jeffrey Thayer and William Bristow for their assistance in evaluating this paper.

References

Axford, W. I., and C. O. Hines, A unifying theory of high-latitude geophysical phenomena and geomagnetic storms, *Can. J. Phys.*, *39*, 1433, 1961.

Banks, P. M., Magnetospheric processes and the behavior of the neutral atmosphere, *J. Geophys. Res.*, *12*, 1051, 1972.

Coroniti, F. V., and C. F. Kennel, Can the ionosphere regulate magnetospheric convection?, *J. Geophys. Res.*, *78*, 2837, 1973.

Crowley, G., J. Schoendorf, R. G. Roble, and F. A. Marcos, Cellular structures in the high-latitude thermosphere, *J. Geophys. Res.*, *101*, 211, 1996.

Deng, W., T. L. Killeen, A. G. Burns, and R. G. Roble, The flywheel effect: Ionospheric currents after a geomagnetic storm, *Geophys. Res. Lett.*, *18*, 1845, 1991.

Deng, W., T. L. Killeen, A. G. Burns, R. G. Roble, J. A. Slavin, and L. E. Wharton, The effects of neutral inertia on ionospheric currents in the high-latitude thermosphere following a geomagnetic storm, *J. Geophys. Res.*, *98*, 7775, 1993.

Emery, B. A., et al., Assimilative mapping of ionospheric electrodynamics in the thermosphere-ionosphere general circulation model comparisons with global ionospheric and thermospheric observations during the GEM/SUNDIAL period of March 28–29, 1992, *J. Geophys. Res.*, *101*, 26,681, 1996.

Fedder, J. A., and J. G. Lyon, The solar wind-magnetosphere-ionosphere current-voltage relationship, *Geophys. Res. Lett.*, *14*, 880, 1987.

Forbes, J. M., and M. Harel, Magnetosphere-thermosphere coupling: An experiment in interactive modeling, *J. Geophys. Res.*, *94*, 2631, 1989.

Goodman, M. L., A three-dimensional, iterative mapping procedure for the implementation of an ionosphere-magnetosphere anisotropic Ohm's law

boundary condition in global magnetohydrodynamic simulations, *Ann. Geophys.*, *13*, 843, 1995.

Groth, C. P. T., D. L. De Zeeuw, T. I. Gombosi, and K. G. Powell, Global 3-D MHD simulation of a space weather event: CME formation, interplanetary propagation, and interaction with the magnetosphere, *J. Geophys. Res.*, *105*, 25,053, 2000.

Heelis, R. A., J. K. Lowell, and R. W. Spiro, A model of the high-latitude ionospheric convection pattern, *J. Geophys. Res.*, *87*, 6339, 1982.

Killeen, T. L., and R. G. Roble, An analysis of the high-latitude thermospheric wind pattern calculated by a thermospheric general circulation model: 1. Momentum forcing, *J. Geophys. Res.*, *89*, 7509, 1984.

Lu, G., A. D. Richmond, B. A. Emery, and R. G. Roble, Magnetosphere-ionosphere-thermosphere coupling: Effect of neutral winds on energy transfer and field-aligned current, *J. Geophys. Res.*, *100*, 19,643, 1995.

Lyons, L. R., T. L. Killeen, and R. L. Walterscheid, The neutral wind "flywheel" as a source of quiet time, polar-cap currents, *Geophys. Res. Lett.*, *12*, 101, 1985.

Moen, J., and A. Brekke, The solar flux influence os quiet-time conductances in the auroral ionosphere, *Geophys. Res. Lett.*, *20*, 971, 1993.

Peymirat, C., A. D. Richmond, B. A. Emery, and R. G. Roble, A magnetosphere-thermosphere-ionosphere electrodynamics general circulation model, *J. Geophys. Res.*, *103*, 17,467, 1998.

Peymirat, C., A. D. Richmond, and R. G. Roble, Neutral wind influence on the electrodynamic coupling between the ionosphere and the magnetosphere, *J. Geophys. Res.*, *107*, 1029, 2002.

Powell, K. G., P. L. Roe, T. J. Linde, T. I. Gombosi, and D. L. De Zeeuw, A solution-adaptive upwind scheme for ideal magnetohydrodynamics, *J. Comp. Phys.*, *154*, 284, 1999.

Richmond, A. D., Ionospheric electrodynamics using magnetic apex coordinates, *J. Geomagn. Geoelectr.*, *47*, 191, 1995a.

Richmond, A. D., The ionospheric wind dynamo: Effects of its coupling with different atmospheric regions, *The Upper Mesosphere and Lower Thermosphere: A Review of Experiment and Theory*, *Geophys. Monogr. Ser.*, vol. 87, edited by R. M. Johnson and T. L. Killeen, p. 49, AGU, Washington, D. C., 1995b.

Richmond, A. D., and Y. Kamide, Mapping electrodynamic features of the high-latitude ionosphere from localized observations: Technique, *J. Geophys. Res.*, *93*, 5741, 1988.

Richmond, A. D., and S. Matsushita, Thermospheric response to a magnetic storm, *J. Geophys. Res.*, *80*, 2839, 1975.

Richmond, A. D., E. C. Ridley, and R. G. Roble, A thermosphere/ionosphere general circulation model with coupled electrodynamics, *Geophys. Res. Lett.*, *19*, 369, 1992.

Ridley, A. J., and M. W. Liemohn, A model-derived stormtime asymmetric ring current driven electric field description, *J. Geophys. Res.*, *107*(A8), 1151, doi:10.1029/2001JA000051, 2002.

Ridley, A. J., C. R. Clauer, G. Lu, and V. O. Papitashvili, A statistical study of the ionospheric convection response to changing interplanetary magnetic field conditions using the assimilative mapping of ionospheric electrodynamics technique, *J. Geophys. Res.*, *103*, 4023, 1998.

Ridley, A. J., G. Crowley, and C. Freitas, A statistical model of the ionospheric electric potential, *Geophys. Res. Lett.*, *27*, 3675, 2000.

Ridley, A. J., D. L. De Zeeuw, T. I. Gombosi, and K. G. Powell, Using steady-state mhd results to predict the global state of the magnetosphere-ionosphere system, *J. Geophys. Res.*, *106*, 30,067, 2001.

Ridley, A. J., K. C. Hansen, G. Tóth, D. L. De Zeeuw, T. I. Gombosi, and K. G. Powell, University of Michigan MHD results of the Geospace Global Circulation Model metrics challenge, *J. Geophys. Res.*, *107*(A10), 1290, doi:10.1029/2001JA000253, 2002.

Robinson, R. M., R. R. Vondrak, K. Miller, T. Dabbs, and D. A. Hardy, On calculating ionospheric conductances from the flux and energy of precipitating electrons, *J. Geophys. Res.*, *92*, 2565, 1987.

Roble, R. G., and E. C. Ridley, An auroral model for the NCAR thermospheric general circulation model (TGCM), *Ann. Geophys.*, *5A*, 369, 1987.

Sánchez, E. R., J. P. Thayer, J. D. Kelly, and R. A. Doe, Energy transfer between the ionosphere and magnetosphere during the January 1997 CME event, *Geophys. Res. Lett.*, *25*, 2597, 1998.

Schoendorf, J., and G. Crowley, Interpretation of an unusal high latitude density decrease in terms of thermospheric density cells, *Geophys. Res. Lett.*, *22*, 3023, 1995.

Song, P., T. I. Gombosi, and A. J. Ridley, Three-fluid Ohm's law, *J. Geophys. Res.*, *106*, 8149, 2001.

Thayer, J. P., Height-resolved Joule heating rates in the high-latitude *E* region and the influence of neutral winds, *J. Geophys. Res.*, *103*, 471, 1998.

Thayer, J. P., and J. F. Vickrey, On the contribution of the thermospheric neutral wind to high-latitude energetics, *Geophys. Res. Lett.*, *19*, 265, 1992.

C. R. Clauer, D. L. De Zeeuw, T. I. Gombosi, and A. J. Ridley, Center for Space Environment Modeling, University of Michigan, Ann Arbor, MI 48109-2143, USA. (rclauer@umich.edu; darrens@umich.edu; tamas@umich.edu; ridley@umich.edu)

A. D. Richmond, High Altitude Observatory, National Center for Atmospheric Research, P. O. Box 3000, Boulder, CO 80307-3000, USA. (richmond@hao.ucar.edu)